

# Modelling realistic horizontal branch morphologies and their impact on spectroscopic ages of unresolved stellar systems

Susan M. Percival<sup>1\*</sup> and Maurizio Salaris<sup>1\*</sup>

<sup>1</sup>*Astrophysics Research Institute, Liverpool John Moores University, Twelve Quays House, Egerton Wharf, Birkenhead CH41 1LD, UK*

## ABSTRACT

The presence of an extended blue horizontal branch (HB) in a stellar population is known to affect the age inferred from spectral fitting to stellar population synthesis models. This is due to the hot blue component which increases the strength of the Balmer lines and can make an old population look spuriously young. However, most population synthesis models still rely on theoretical isochrones which do not include realistic modelling of extended HBs. In this work, we create detailed models for a range of old simple stellar populations (SSPs), with metallicities ranging from  $[\text{Fe}/\text{H}] = -1.3$  to solar, to create a variety of realistic HB morphologies, from extended red clumps, to extreme blue HBs. We achieve this by utilising stellar tracks from the BaSTI database and implementing a different mass loss prescription for each SSP created. This includes setting an average mass and a Gaussian spread in masses of individual stars coming on to the zero age HB for each model, and hence resulting in different HB morphologies. We find that, for each metallicity, there is some HB morphology which maximises  $H\beta$ , making an underlying 14 Gyr population look  $\sim 5 - 6$  Gyr old for the low and intermediate metallicity cases, and as young as 2 Gyr in the case of the solar metallicity SSP. We explore whether there are any spectral indices capable of breaking the degeneracy between an old SSP with extended blue HB and a truly young or intermediate age SSP, and find that the  $\text{CaII}$  index of Rose (1984) and the strength of the  $\text{MgII}$  doublet at  $2800\text{\AA}$  are promising candidates, in combination with  $H\beta$  and other metallicity indicators such as  $\text{Mg}b$  and  $\text{Fe}5406$ . We also run Monte Carlo simulations to investigate the level of statistical fluctuations in the spectra of typical stellar clusters. We find that fluctuations in spectral indices are significant even for average to large globular clusters, and that various spectral indices are affected in different ways, which has implications for full-spectrum fitting methods. Hence we urge caution if these types of stellar clusters are to be used as empirical calibrating objects for various aspects of SPS models.

**Key words:** stars: horizontal branch – globular clusters: general – galaxies: stellar content.

## 1 INTRODUCTION

In recent years, stellar population synthesis (SPS) models have rapidly become a fundamental tool in the study of both Galactic and extragalactic stellar populations (see Percival et al. 2009; Kotulla et al. 2009; Coelho et al. 2007; Vázquez & Leitherer 2005; Maraston 2005; Bruzual & Charlot 2003 for some recent examples). Despite the increasing sophistication of the underlying stellar models used in SPS and ever-growing libraries of spectra (both empirical and synthetic) available to modellers,

there are still areas in which models, and methods for fitting them to observational data, can be significantly improved and expanded. Some of the current shortcomings are due to the need to adopt simplifying assumptions about the stellar population in question in order to make some problems tractable, e.g. the fitting of simple stellar population (SSP) models to galaxies, assuming that they can be represented by a single age, single metallicity model.

A key area in which simplifying assumptions are implicitly made is the morphology of the horizontal branch (HB) for individual SSPs – this is largely due to the limitations of theoretical isochrones, which are used as the basis of all SPS models (except those of Maraston and co-workers,

\* E-mail: smp@astro.livjm.ac.uk ; ms@astro.livjm.ac.uk

who use a fuel-consumption based method – see Maraston 2005 and references therein). However it is well known that the morphology of the HB can impact strongly on the integrated light of stellar populations especially if an extended blue component is present, potentially affecting both colours and line indices, and hence impacting on inferred ages for these systems (see e.g. Ocvirk 2010; Conroy et al. 2009; Schiavon et al. 2004; Lee et al. 2002, 2000). Hence it is vital to assess the ways which these ‘simplified’ HBs inherent in theoretical isochrones impact on SPS models, and whether a more realistic and detailed treatment of the HB is necessary, or indeed practical. This is the purpose of the work presented here.

For unresolved stellar populations our knowledge of their ages and elemental abundances is largely derived through the fitting of diagnostic spectral indices, hence the focus of our work is to investigate the effect of a detailed treatment of the HB on key spectral indices, such as  $H\beta$ . However, it is important to realise that our results will also impact on analyses which use full-spectrum fitting methods, as will be discussed in Section 5.

In real stellar systems the horizontal extension of the HB is governed by stochastic mass loss in stars approaching the tip of the red giant branch (TRGB). All the stars in a particular SSP leave the TRGB with the same core mass but individual stars have different masses remaining in the outer layers, which determine the position of the star along the zero-age horizontal branch (ZAHB). In stellar models this mass loss is parameterised by the mass loss parameter,  $\eta$ , which is assigned some fixed value calculated according to the Reimers mass loss relation (Reimers 1975). Hence in theoretical isochrones the HB comprises a single mass point, with no extension.

It is worth remembering here that an isochrone consists of a series of evolutionary points (EPs) which define the locus of points for an SSP. Whilst each EP defines the appropriate stellar parameters for any star located at that point, in terms of mass, effective temperature and luminosity, they do not represent individual stars themselves. In order to create an SSP, an isochrone is “populated” according to some initial mass function (IMF) which effectively gives the appropriate weighting to each EP. In most population synthesis work the isochrone is treated as an analytical function for this purpose, so that all EPs along the isochrone are smoothly populated and the ZAHB remains as a single mass point. In order to create a model with an extended HB, effectively incorporating a spread in mass loss, the isochrone (or, at least, the HB portion) must be populated with a discrete number of stars, so that each star in the HB phase can be assigned a specific mass from within some range of masses – this requires interpolation between individual core-helium burning stellar tracks.

Creating an integrated spectrum for these extended HB models is a computationally expensive procedure since the time taken is proportional to the number of points in the simulation (for details on how integrated spectra for SSPs are produced the interested reader is referred to Percival et al. 2009, hereafter P09). For the analytical case, the number of points is just the number of EPs along the isochrone, which varies between a few hundred and around two thousand depending on which isochrone set is used. To populate an isochrone with individual stars, one has to con-

sider the problem of statistical fluctuations which are likely to arise as a result of low numbers of stars (and hence poor sampling) in the later stages of evolution, including the HB phase. This is of particular relevance in the case of an SSP with an extended blue HB, since these hot blue HB stars give rise to strong Balmer lines, which are generally used as the primary age indicators for stellar populations. This problem can only be overcome by using large numbers of points in the simulation, potentially up to  $\sim 10^6$ . In fact, part of the work presented here is to explore how large these statistical fluctuations can be in real stellar clusters, and how many input stars are needed in the models to avoid significant uncertainties in ages and metallicities derived from the final integrated SSP spectra.

Another problem in creating models with extended HBs is that there is still no theory which predicts mass loss rates from stellar parameters and so the value of  $\eta$  is chosen arbitrarily, usually to reflect the typical HBs seen in Galactic globular clusters. This is complicated by the fact that clusters apparently with the same age and chemical composition can have different HB morphologies. However, in principle  $\eta$  can take any value and so producing a database of SPS models to cover all possibilities is not feasible.

The pioneering work of Lee et al. (2000) (hereafter L2000) highlighted the importance of including realistic HBs in stellar population work. L2000 created models for 15 SSPs using a single value for the mass loss parameter for all their models, which was chosen to replicate the range of HBs seen in Galactic globular clusters. They included a Gaussian spread in the HB mass distribution of  $\sigma_M = 0.02 M_\odot$  to simulate the observed extension of the HB. This work graphically demonstrated the systematic variation of HB morphology with age and metallicity (see their Figure 5), showing that, at fixed  $\eta$ , HBs generally become bluer as metallicity decreases and as age increases. L2000 note that the strength of the  $H\beta$  line in the integrated population does not increase monotonically as metallicity decreases at a fixed age, but peaks at some intermediate metallicity and then falls again as metallicity continues to decrease. This is because  $H\beta$  reaches a maximum strength in stellar spectra when the effective temperature,  $T_{eff}$ , is around 9500K and so  $H\beta$  is maximised if the distribution of stars along the HB centres around this value. In these cases the contribution to  $H\beta$  from the HB completely dominates over the contribution from the main-sequence turnoff and makes the population look spuriously young.

It is apparent from the L2000 figures, but not specifically noted by them, that the actual extension (i.e. from red to blue) of the HB in the colour-magnitude diagrams is very different for the various SSPs, even though the value of  $\eta$  and  $\sigma_M$  are the same. This is because the stellar effective temperature in this phase is extremely sensitive to very small changes in envelope mass and so the resulting HB morphologies can be very different, even when the same mass loss prescription is used.

In this paper we use similar techniques to L2000 to model extended HBs, populating them with discrete numbers of stars by interpolating between core-helium burning stellar tracks and using a Gaussian spread in the mass loss distribution, and we extend that work in 3 key ways. Firstly we explore the effects of varying  $\eta$  at fixed age and metallicity, which enables us to model high mass loss in metal

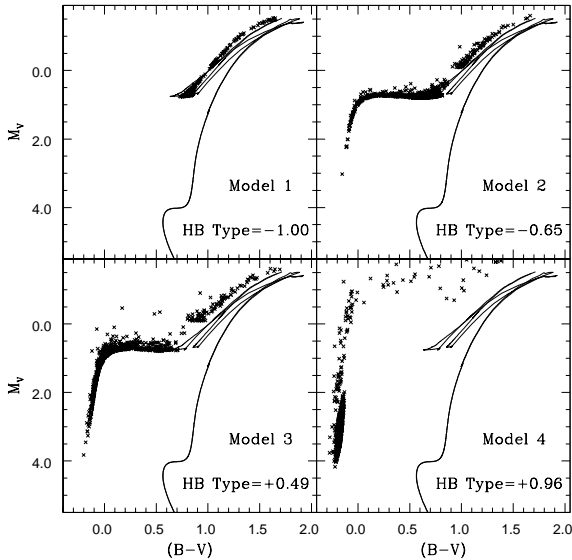


**Figure 1.** 4 models from the  $\alpha$ -enhanced,  $[\text{Fe}/\text{H}] = -0.70$  set. For clarity, only 500 points are plotted for each HB ( $\sim 10000$  were used in each simulation). The 14 Gyr isochrone used for the underlying population up to the TRGB is also plotted. For reference purposes, the later evolutionary stages of the isochrone are also shown for the 2 ‘standard’ cases in the BaSTI database, i.e. with fixed  $\eta = 0.2$  and  $\eta = 0.4$ . Horizontal branch morphology is parameterised by  $\text{HB type} = (B - R)/(B + V + R)$  – see text for details.

rich systems to see whether we can mimic a system such as M32, which has approximately solar metallicity, but an extended blue HB component. We are also able to create SSPs at different metallicities with bimodal HBs, similar to those observed in several Galactic globular clusters. Secondly, we create several models which we populate with numbers of stars representative of typical stellar clusters, and use Monte Carlo techniques to explore the impact of statistical fluctuations on measured diagnostic line indices, such as  $H\beta$ . Thirdly, we create full integrated high resolution spectra for all our models and simulations which enables us to assess the behaviour of all diagnostic line indices (within a wavelength range  $2500\text{\AA}$  to  $\sim 6000\text{\AA}$ ), as well as the continuum flux. We also investigate whether there are any diagnostic indices capable of breaking the degeneracy between an old SSP with extended blue HB (hence strong  $H\beta$ ) and a truly young or intermediate age SSP.

## 2 MODELLING SSPS WITH EXTENDED HORIZONTAL BRANCHES

### 2.1 Method

As a starting point, we created 16 SSPs with extended HBs, in 4 sets of 4 models each: these comprise 2 sets with scaled-solar abundance ratios, at  $[\text{Fe}/\text{H}] = -1.27, +0.06$  (solar metallicity) and 2 sets with  $\alpha$ -enhanced ratios, at  $[\text{Fe}/\text{H}] = -1.31, -0.70$ . In each case the underlying population was created from an appropriate metallicity 14 Gyr isochrone

**Table 1.** Parameters used for  $\alpha$ -enhanced HB models.

| Model | $[\text{Fe}/\text{H}]$ | $\langle M \rangle (M_\odot)$ | $\sigma_M$ |
|-------|------------------------|-------------------------------|------------|
| 1     | -1.31                  | 0.70                          | 0.02       |
| 2     | -1.31                  | 0.64                          | 0.03       |
| 3     | -1.31                  | 0.58                          | 0.03       |
| 4     | -1.31                  | 0.51                          | 0.005      |
| 1     | -0.70                  | 0.71                          | 0.02       |
| 2     | -0.70                  | 0.60                          | 0.03       |
| 3     | -0.70                  | 0.55                          | 0.02       |
| 4     | -0.70                  | 0.495                         | 0.005      |

**Table 2.** Parameters used for scaled-solar HB models.

| Model | $[\text{Fe}/\text{H}]$ | $\langle M \rangle (M_\odot)$ | $\sigma_M$ |
|-------|------------------------|-------------------------------|------------|
| 1     | -1.27                  | 0.72                          | 0.02       |
| 2     | -1.27                  | 0.65                          | 0.02       |
| 3     | -1.27                  | 0.58                          | 0.02       |
| 4     | -1.27                  | 0.53                          | 0.01       |
| 1     | +0.06                  | 0.70                          | 0.03       |
| 2     | +0.06                  | 0.63                          | 0.03       |
| 3     | +0.06                  | 0.56                          | 0.02       |
| 4     | +0.06                  | 0.51                          | 0.01       |

from the BaSTI database<sup>1</sup> (Pietrinferni et al. 2004, 2006). For each model the isochrone was populated analytically up to the TRGB and the integrated spectrum for this portion of the isochrone was created using high resolution spectra from Munari et al. (2005), as described in P09. The HB was treated separately and populated with a large number of individual points ( $> 10000$ , in order to avoid the problem of statistical fluctuations) with some mean mass (corresponding to some value of  $\eta$ ), and with a Gaussian spread in the mass distribution,  $\sigma_M$ , by interpolating between core-helium burning stellar tracks. Spectra were assigned to each point in the HB simulation as usual, i.e. matching  $T_{\text{eff}}$ ,  $\log g$ , and  $[\text{Fe}/\text{H}]$ , and these were then summed together. The summed HB spectrum was then scaled appropriately before being added to the spectrum of the underlying population to create the final integrated spectrum for each model.

Equivalent widths of various diagnostic line indices were measured on the resulting integrated spectra, as described in P09, so that comparisons could be made with the BaSTI SPS database. Briefly, the line indices discussed here are from the Lick/IDS bandpasses tabulated in Trager et al. (1998), unless otherwise stated. The quoted line strengths were obtained using the LECTOR programme by A. Vazdekis<sup>2</sup> and are those directly measured on the spectra, i.e. they are *not* transformed onto the Lick system. We focus in particular on the  $H\beta$  index in the following section since it is used primarily as an age indicator for SSPs.

In each set of models, the 4 cases were created to approximately match the extremes of HBs seen in Galactic globular clusters, from a purely red, but extended HB (i.e. a red clump – HB model 1) to an extremely blue HB with extended blue tail (HB model 4), plus 2 intermediate cases

<sup>1</sup> Available at <http://albione.oa-teramo.inaf.it/>

<sup>2</sup> See <http://www.iac.es/galeria/vazdekis/index.html>

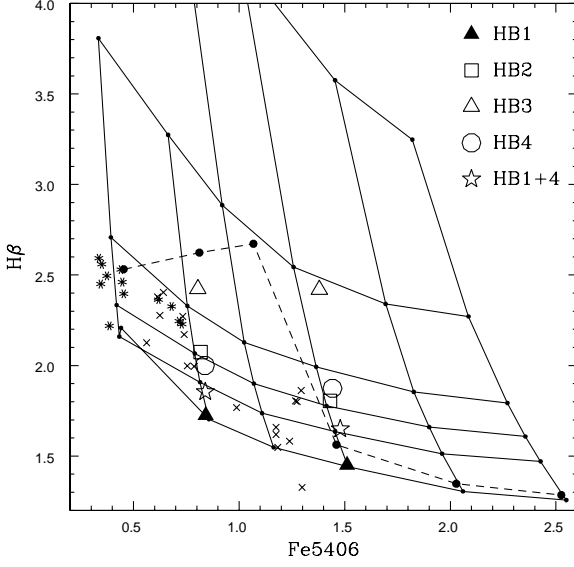


**Figure 2.**  $H\beta$  vs. Fe5406  $\alpha$ -enhanced grid with results for the 2 sets of  $\alpha$ -enhanced models overplotted. The underlying grid is from the BaSTI SPS database, with fixed  $\eta = 0.2$ , for SSP ages 1.25, 3, 6, 8, 10 and 14 Gyr (from top to bottom) and  $[\text{Fe}/\text{H}] = -1.84, -1.31, -1.01, -0.70, -0.29, +0.05$  (increasing from left to right). The dashed line is for the 14 Gyr BaSTI SSPs with fixed  $\eta = 0.4$ . Crosses and asterisks are observational data for Galactic GCs from Schiavon et al. (2005) – the asterisks denote clusters with HB type  $> 0.8$  (i.e. predominantly blue).

(HB models 2 and 3). We also combined spectra from the extreme red and extreme blue cases to create models with a bi-modal HB. Parameters used for each set of models, in terms of metallicity, mean mass  $\langle M \rangle$ , and  $\sigma_M$ , are tabulated in Tables 1 and 2, respectively, for the  $\alpha$ -enhanced and scaled-solar sets.

Figure 1 shows the  $V/(B-V)$  colour magnitude diagrams (CMDs) for the  $\alpha$ -enhanced,  $[\text{Fe}/\text{H}] = -0.70$  set of 4 models, which illustrates the typical HB morphologies for each set. The HB morphological type  $(B-R)/(B+V+R)$ , as defined in Lee et al. (1994), was calculated using the boundaries of the instability strip defined in Cordier et al. (2007), and is notated on each plot. The appropriate isochrone (used to create the underlying population up to the TRGB) is also plotted for the 2 ‘standard’ cases in the BaSTI database, i.e. with fixed  $\eta$  of 0.2 and 0.4. At this intermediate metallicity the ZAHBs for the  $\eta=0.2$  and  $\eta=0.4$  cases have similar effective temperature, hence there is only a small difference in their location in the CMD. The  $\eta=0.4$  case always produces a hotter (i.e. bluer) ZAHB than the  $\eta=0.2$  one, but for metallicities of  $[\text{Fe}/\text{H}] \sim -0.70$  and greater, this still produces a ZAHB which is cooler (i.e. redder) than the turn off (TO), even at old ages. However, for metallicities lower than this, at old ages, the  $\eta=0.4$  case produces a ZAHB which is very different from the  $\eta=0.2$  case, and is much hotter (bluer) than the TO. The difference between the 2 cases, and the impact on derived ages, is discussed in Section 2.2.

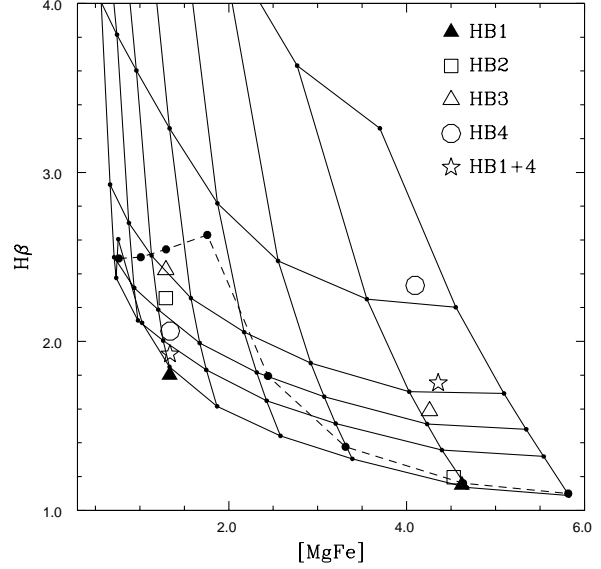


**Figure 3.**  $H\beta$  vs.  $[\text{MgFe}]$  scaled-solar grid with results for the 2 sets of scaled-solar models overplotted. The underlying grid is as in Figure 2 but for  $[\text{Fe}/\text{H}] = -1.79, -1.49, -1.27, -0.96, -0.66, -0.35, +0.06, +0.40$ .

## 2.2 Results

Figure 2 shows results from the  $\alpha$ -enhanced HB models in the  $H\beta$  v. Fe5406 diagnostic grid, i.e. where  $H\beta$  is the age indicator and Fe5406 traces iron abundance,  $[\text{Fe}/\text{H}]$ . Similarly, Figure 3 shows results from the scaled-solar HB models in the  $H\beta$  vs.  $[\text{MgFe}]$  grid, where  $[\text{MgFe}]$  is a tracer of total metallicity,  $Z$  (see P09). In these figures, HB1 refers to the red clump only HB model, HB4 refers to the extended blue tail case and HB2 and HB3 are the intermediate cases. The underlying models from which these grids are constructed are the BaSTI  $\eta=0.2$  models (solid lines), with the  $\eta=0.4$  models at 14 Gyr only overlaid (dashed lines), described in P09.

Before discussing the results of the extended HB simulations it is important to note the behaviour of  $H\beta$  in the fixed  $\eta=0.4$  models, at old ages, compared to the  $\eta=0.2$  ones. Figures 2 and 3 clearly demonstrate that at metallicities above  $[\text{Fe}/\text{H}] \sim -0.7$ , the  $H\beta$  line has similar strength for the 2 cases, indicating that their HBs have similar average temperatures and both appear as red clumps in a CMD. However between  $[\text{Fe}/\text{H}] = -0.7$  and  $[\text{Fe}/\text{H}] = -1.0$ , the  $H\beta$  line suddenly becomes much stronger for the  $\eta=0.4$  case, which is an indication that the HB stars are much hotter than for the  $\eta=0.2$  case, and hence the HB would appear much bluer than the turn off in a CMD. For the  $\eta=0.4$  models,  $H\beta$  peaks at a metallicity of around  $[\text{Fe}/\text{H}] = -1.0$  and then decreases again as the metallicity continues to decrease. This is the same behaviour noted by L2000 and happens because the average temperature of the HB stars gets increasingly hot as the metallicity decreases until it is significantly hotter than 9500K (where the  $H\beta$  strength peaks).

In all 4 model sets, an extended red only HB (model HB1) only negligibly affects  $H\beta$  compared to the ‘standard’ BaSTI SSP model with single mass ZAHB and  $\eta=0.2$ , hence

the inferred age from these diagnostic grids is the correct one for the underlying stellar population, i.e. 14 Gyrs. For the 3 sets of models with sub-solar metallicity (i.e. the 2  $\alpha$ -enhanced sets and one of the scaled-solar sets),  $H\beta$  reaches a peak for one of the intermediate morphology cases (model HB3), and is similar to the fixed  $\eta=0.4$  case, whilst for the scaled-solar solar metallicity set,  $H\beta$  peaks for model HB4, i.e. the extended blue tail case. For the lower metallicity models, at  $[Fe/H] \sim -1.3$ , the peak in  $H\beta$ , whether from the extended HB model or from the fixed  $\eta=0.4$  case, implies an age around 5-6 Gyrs, whilst for the solar metallicity case the inferred age is  $<3$  Gyr (remembering that the underlying population is a 14 Gyr one in all cases.)

Looking in more detail at the individual models, it is evident that if a particular HB simulation has a distribution with a mean mass which corresponds to  $T_{eff} \sim 9000-9500K$ , then  $H\beta$  is maximised, implying spuriously young ages from the integrated SSP spectra (confirming the result noted by Lee et al. 2000).

We created bi-modal HBs by combining models HB1 and HB4 in each set, and varying the fractions of the red and blue components. In all cases it was found that the change in  $H\beta$  strength just scales linearly with the change in blue HB fraction. This is illustrated in Figures 2 and 3 where the open star symbol represents the 50/50 case (i.e. 50% red, 50% blue HB) which always lies exactly half way between model HB1 and model HB4. Therefore inferred ages for an underlying 14 Gyr population can lie anywhere between  $<3$  and 14 Gyr depending on the precise details of the HB morphology and the metallicity of the population.

In general, the measured EWs of the various metal lines are only marginally affected by the HB extension, however inferred metallicities can still change if  $H\beta$  increases significantly, since none of the diagnostic grids is completely orthogonal. In practice however, these inferred changes in metallicity are likely to be within the observational errors in most cases.

### 3 IDENTIFYING EXTENDED BLUE HB TRACERS

One of the main issues raised by the results presented here is whether there are any diagnostic indices which could potentially distinguish between an old population with an extended blue HB and a simple, single-aged population with an intermediate age (between, say, 3 and 8 Gyrs) in the integrated spectrum of an unresolved stellar system. This point has been raised before, but generally in the context of Galactic globular clusters, which all have sub-solar metal abundances and where it is known from isochrone fitting that the true ages are  $>10$  Gyr. Here we demonstrate quite clearly that any old population, even at solar and super-solar metallicities, can have a hot HB if there is sufficient mass loss (coupled with a spread in mass loss) on the RGB, and that this will have the effect of making that population look spuriously young when deriving ages from Balmer lines. This is not merely an academic point since it is known that the compact elliptical galaxy M32, which has near solar metallicity, has just such an extended blue HB component, which appears to centre around 9000-10000K (Brown & Ferguson 2003), the temperature at which the  $H\beta$  line is strongest. It

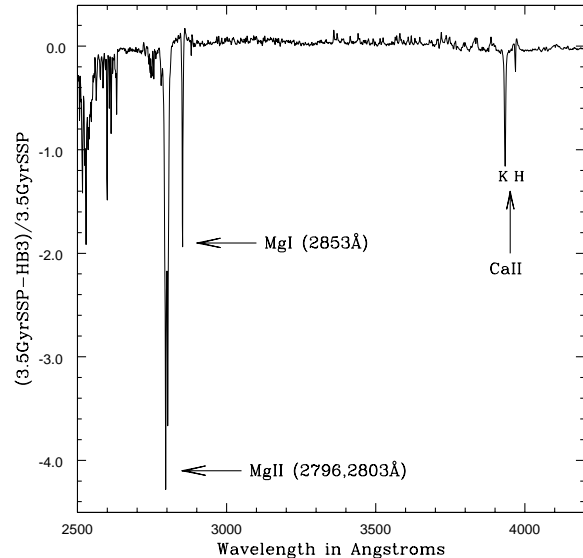


**Figure 4.** Fractional difference spectrum between HB model 3 (14 Gyr plus extended blue HB) and a 3.5 Gyr SSP with  $\eta=0.2$ , from the  $\alpha$ -enhanced,  $[Fe/H]=-0.7$  set of models. Spectra were normalised at 6000Å.

is not clear what fraction of the total population contributes to this blue HB as this is difficult to quantify from observational data, but it is known that the spectroscopic age of M32, from its Balmer lines, is around 3 Gyr (Schiavon et al. 2004).

In order to help in the identification of potentially discriminating features in the spectra, we compared the integrated spectrum of the HB model 3 case (14 Gyr, with an extended blue HB, maximising  $H\beta$ ) with a 3.5 Gyr SSP at the same metallicity. We used the  $\alpha$ -enhanced,  $[Fe/H]=-0.7$  set of models for this purpose. It can be seen from Figure 2 that the  $H\beta$  and Fe5406 index strengths are almost exactly the same for the 2 scenarios, as indeed are the strengths of other metal indicators such as Mg b and the various Fe lines (not illustrated here). The flux for the 2 spectra was normalised to unity at 6000Å and a fractional difference calculated in the sense  $(3.5GyrSSP - HBmodel3)/3.5GyrSSP$ . The resulting fractional difference spectrum is shown in Figure 4 which shows that all the differences between the 2 cases lie at wavelengths shorter than  $\sim 4000\text{\AA}$  and, in fact, longwards of 4500Å this difference spectrum is almost featureless. The 3 features which obviously stand out are the CaII feature made up of the H and K lines (3968.5Å and 3933.7Å), MgI (2853Å) and the MgII doublet (2796Å and 2803Å). It is also clear that the continuum levels shortward of the magnesium features are different in the sense that the 14 Gyr population with extended blue HB has stronger UV continuum than the 3.5 Gyr population.

We note here that we also performed a similar test for the solar metallicity, scaled solar models, comparing the spectrum of HB model 4 with a 3 Gyr SSP at the same metallicity, and found quantitatively very similar results to the  $\alpha$ -enhanced case described above.

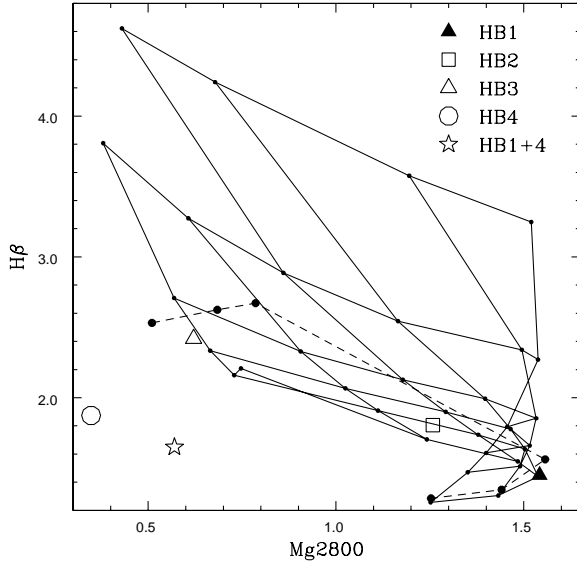


**Figure 5.**  $H\beta$  vs.  $Mg2800$   $\alpha$ -enhanced grid. The underlying grid, model datapoints and symbols are as for Figure 2 – only the  $[Fe/H]=-0.7$  set of models is shown, for clarity.

### 3.1 The $MgII$ index

At first glance it appears that the  $MgII$  feature around  $2800\text{\AA}$  is the most obvious candidate to investigate as an extended blue HB discriminator. This index, which is measured as an equivalent width, was defined by Fanelli et al. (1990) who were looking for temperature, luminosity, and metallicity discriminants for stellar spectra in the mid-UV. They found  $MgII$  displays “no sensitivity to abundance for cool stars and a reversed sensitivity in FG dwarfs such that metal-poor stars have stronger  $MgII$  strengths at the same temperature than more metal-rich stars”. We calculated the  $MgII$  equivalent widths from the integrated spectra of all the models created here, as well as for the BaSTI  $\eta=0.2$  and  $\eta=0.4$  models used for our underlying grids. The resulting  $H\beta$  vs.  $MgII$   $\alpha$ -enhanced diagram is shown in Figure 5 (for clarity, only the HB model set at  $[Fe/H]=-0.7$  is plotted). This grid clearly shows the behaviour referred to by Fanelli et al. (1990) as the higher metallicity end of the grid (i.e. towards the right of the diagram) folds back on itself, so that there is a large degree of degeneracy at old ages for all metallicities above  $[Fe/H]\sim -1.0$ , at least for the fixed  $\eta=0.2$  case.

More promisingly, there is a strong trend towards lower  $MgII$  values as the HBs become more extended towards the blue. Figure 5 shows that the HB models 3 and 4 lie outside the standard grid, implying a much lower metallicity than the true one. However, because the grid is not very orthogonal, the implied age is actually close to the true age of 14 Gyr. Interestingly the Lick index  $Mgb$  behaves similarly to the Fe and  $[Mg/Fe]$  indices displayed in Figures 2 and 3, i.e. it is negligibly affected by extended blue HBs, and so this index *does* give a good indication of the true metallicity. Hence any discrepancy between the implied metallicities from the  $Mgb$  and  $MgII$  indices for a given stellar population could be due to the presence of an extended blue HB component.

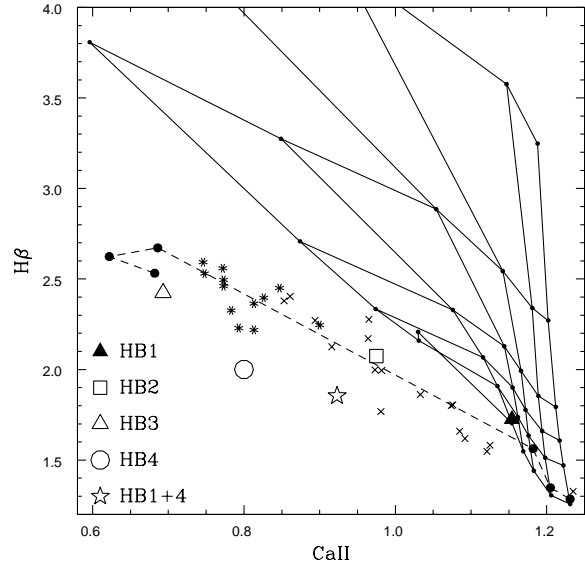


**Figure 6.**  $H\beta$  vs.  $CaII$   $\alpha$ -enhanced grid. The underlying grid, model datapoints and symbols are as for Figure 2 – only the  $[Fe/H]=-1.3$  set of models is shown, for clarity. Crosses and asterisks are observational data for Galactic GCs from Schiavon et al. (2005) – the asterisks denote clusters with HB type  $> 0.8$  (i.e. predominantly blue).

There is tentative evidence that  $MgII$  could be used in this way in the UV data presented in Ponder et al. (1998). Their Table 4 includes  $MgII$  data for several Galactic GCs, including the well known pair M3 (NGC 5272) and M13 (NGC 6205), which are known to have almost identical metallicities (around  $[Fe/H]=-1.5$ ) and similar ages, to within  $\sim 1$  Gyr. However their HB morphologies are quite different, with that of M13 having a very extended blue tail. The Ponder et al. (1998) data show that their  $MgII$  strengths are different by 0.26 in the sense that M13 value is lower, which is qualitatively and quantitatively in reasonable agreement with our predictions.

An important caveat to the behaviour of  $MgII$  discussed here is that the current version of our population synthesis models does not include post-AGB stars, which are expected to emit much of their flux at UV wavelengths. Whilst an order of magnitude estimate indicates that their contribution to the continuum flux of an integrated spectrum is likely to be very small, it would be unwise to assume that they would not affect line indices. However, this magnesium feature is clearly an intriguing possibility and merits further investigation.

### 3.2 The $CaII$ index

The  $CaII$  index was identified by Rose (1984) as being highly sensitive to the presence of A stars in a composite spectrum. This index is constructed by dividing the central intensity of the  $CaII$  H + H $\epsilon$  line by the central intensity of the  $CaII$  K line. Rose (1984) states that “this ratio, which is constant in F, G, and K stars, decreases dramatically in A and B stars as the  $CaII$  lines weaken and H $\epsilon$  strengthens”. Since A stars have effective temperatures in the range 8000K–

10000K, which encompasses the range of the extended blue HB stars of interest here, this index merits a more detailed analysis. Hence we calculated  $\text{CaII H} + \text{H}\epsilon/\text{CaII K}$  from the integrated spectra of all the models created here, as well as for the BaSTI  $\eta=0.2$  and  $\eta=0.4$  models used for our underlying grids. The resulting  $\text{H}\beta$  vs.  $\text{CaII } \alpha$ -enhanced grid is shown in Figure 6 (for clarity, only the HB model set at  $[\text{Fe}/\text{H}]=-1.3$  is plotted).

The first striking feature of this plot is that the lower metallicity 14 Gyr SSPs with  $\eta=0.4$  (the dashed line) lie outside the  $\eta=0.2$  grid. Compare this with the  $\text{H}\beta$  vs.  $\text{Fe5406}$  grid in Figure 2, and the  $\text{H}\beta$  vs.  $\text{Mgb}$  grid in Figure 5, where the  $\eta=0.4$  models lie completely within the  $\eta=0.2$  grid. Perhaps more importantly, all the extended HB models also lie outside the  $\eta=0.2$  grid, except for HB model 1, which is the red clump case which has no blue component (and thus behaves very similarly to the fixed  $\eta=0.2$  case). This means that the combination of  $\text{H}\beta$  and the  $\text{CaII}$  index could potentially distinguish between an old population with extended blue HB and an intermediate age or young SSP. Overplotted on Figure 6 are Galactic globular cluster data from Schiavon et al. (2005) for which we have measured the indices directly on the observed spectra in exactly the same way as for our models. It is interesting to note that these clusters, which all have sub-solar metallicity and extended HBs, all lie in the region of the diagram covered by our extended HB models. In fact, closer inspection of individual clusters reveals that the clusters with the bluest HBs do indeed fall towards the left hand side of this diagram, with lower  $\text{CaII}$  values. Clusters with HB type  $> 0.8$  (i.e. predominantly blue) have been plotted as asterisks and it can be seen that they all fall well outside the fixed  $\eta=0.2$  ‘standard’ grid. Looking again at the  $\text{H}\beta$  vs.  $\text{Fe5406}$  grid in Figure 2 it can be seen that these same blue HB clusters would all appear to have ages around 6-7 Gyr in that plane. If their strong  $\text{H}\beta$  was really being caused by younger ages rather than blue HBs, then these clusters would have a higher  $\text{CaII}$  ratio for the same  $\text{H}\beta$  strength and the points would lie further towards the right in the  $\text{H}\beta$  vs.  $\text{CaII}$  grid.

An important caveat to note regarding the  $\text{CaII}$  index is that it is strongly affected by velocity dispersion, and also requires very high signal-to-noise data. This is because it is measured simply as the ratio of the depths at the central points of the Ca H and K lines, and is not an equivalent width (or magnitude) as most of the other diagnostic indices in general use are. This means it is not an ideal choice for studying elliptical galaxies, unless their velocity dispersions are known to be low. However it may be a useful indicator for application to extragalactic globular clusters, if sufficiently high signal-to-noise spectra can be obtained to measure the relative depths of the Ca lines accurately. Further issues relating to the  $\text{CaII}$  index and its use are discussed in Section 5.

## 4 STATISTICAL FLUCTUATIONS TESTS

### 4.1 Method

In order to assess the likely impact of statistical fluctuations on integrated spectra, and hence diagnostic line indices, for real stellar systems, we simulated 2 cases representing typical Galactic globular clusters (GCs). These 2 cases were

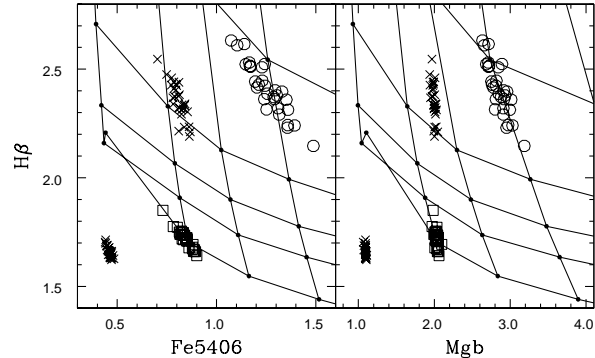


**Figure 7.** Diagnostic grids with results from 30 realisations of each of the 3 models described in the text (lines of constant age and  $[\text{Fe}/\text{H}]$  are as in Figure 2):  $2 \times 10^5 M_{\odot}$  GC with HB model 1 (*open squares*);  $2 \times 10^5 M_{\odot}$  GC with HB model 3 (*crosses*);  $2 \times 10^4 M_{\odot}$  open cluster with HB model 1 (*open circles*). Data points in the lower left of each diagram are 30 realisations of the GC with HB model 3 modelled using  $2 \times 10^6 M_{\odot}$ , which have been shifted arbitrarily for clarity – as measured they are centred on the same location as the  $2 \times 10^5 M_{\odot}$  data.

based on the 14 Gyr,  $[\text{Fe}/\text{H}]=-1.31$  ( $\alpha$ -enhanced) SSP set of models listed in Table 1. Specifically we used Model 1 and Model 3 as the basis for these simulations, which are, respectively, the red clump HB case which does not significantly affect  $\text{H}\beta$ , and the intermediate extension HB case, which results in the  $\text{H}\beta$  peak seen in Figure 2. For these tests, the whole of the underlying isochrone up to the TRGB, plus the extended HB, were populated with a discrete number of stars to represent a total cluster mass of  $2 \times 10^5 M_{\odot}$ . For individual points along the RGB the mass loss was varied to give a spread of masses on the HB and hence a horizontal extension, as described in Section 2.1.

We also modelled a representative low mass cluster using a 3.5 Gyr,  $[\text{Fe}/\text{H}]=-0.7$  SSP as the underlying population, for which we adopted a total cluster mass of  $2 \times 10^4 M_{\odot}$ . These parameters were chosen to simulate a stellar cluster typical of those found in the Magellanic Clouds, such as those studied in Dias et al. (2010). The reasons for this choice will be discussed further in Section 5. Observationally, this type of cluster would typically have a red clump HB (model 1) which, although extended rather than fixed point, is negligibly different from the fixed  $\eta=0.2$  case (as demonstrated in Section 2.2).

For all 3 of these systems, we ran Monte Carlo simulations, creating 30 realisations of each case. To explore the likely maximum mass at which statistical fluctuations might be significant in stellar clusters, we also created 30 realisations of the 14 Gyr extended blue HB case adopting a cluster mass of  $2 \times 10^6 M_{\odot}$ .

**Table 3.**  $1\sigma$  variations in 21 Lick indices, plus  $H\delta_F$ ,  $H\gamma_F$  and  $CaII$ , from the (30) extended blue HB simulations at  $2 \times 10^5 M_\odot$ .

| Index       | $1\sigma$ | Units        |
|-------------|-----------|--------------|
| $H\delta_F$ | 0.129     | $\text{\AA}$ |
| $H\gamma_F$ | 0.143     | $\text{\AA}$ |
| $CN_1$      | 0.003     | mag          |
| $CN_2$      | 0.003     | mag          |
| $Ca4227$    | 0.028     | $\text{\AA}$ |
| $G4300$     | 0.134     | $\text{\AA}$ |
| $Fe4383$    | 0.091     | $\text{\AA}$ |
| $Ca4455$    | 0.028     | $\text{\AA}$ |
| $Fe4531$    | 0.069     | $\text{\AA}$ |
| $C24668$    | 0.042     | $\text{\AA}$ |
| $H\beta$    | 0.084     | $\text{\AA}$ |
| $Fe5015$    | 0.106     | $\text{\AA}$ |
| $Mg_1$      | 0.003     | mag          |
| $Mg_2$      | 0.004     | mag          |
| $Mgb$       | 0.024     | $\text{\AA}$ |
| $Fe5270$    | 0.054     | $\text{\AA}$ |
| $Fe5335$    | 0.057     | $\text{\AA}$ |
| $Fe5406$    | 0.035     | $\text{\AA}$ |
| $Fe5709$    | 0.032     | $\text{\AA}$ |
| $Fe5782$    | 0.017     | $\text{\AA}$ |
| $Na\ D$     | 0.027     | $\text{\AA}$ |
| $TiO_1$     | 0.001     | mag          |
| $TiO_2$     | 0.001     | mag          |
| $CaII$      | 0.015     | –            |

## 4.2 Results

Results from the statistical fluctuation tests are displayed in Figure 7 which shows the  $H\beta$  vs.  $Fe5406$  and  $H\beta$  vs.  $Mgb$  diagnostic grids. For the  $2 \times 10^5 M_\odot$  GC simulations the scatter in  $H\beta$  is significant, and is larger for the extended blue HB case. However it is difficult to rigorously quantify the impact on implied ages for 3 reasons. Firstly, for the same degree of scatter in  $H\beta$ , the scatter in apparent age depends on the absolute  $H\beta$  strength, since  $H\beta$  strength does not vary linearly with age. For example, a change of  $\pm 0.2$  in  $H\beta$  implies a shift of  $\sim 1$  Gyr for a 3 Gyr SSP, but a shift of  $\sim 4$  Gyr for a 12 Gyr SSP. Secondly, for the extended blue HB case, the implied age is dominated by the large offset towards younger ages caused by the blue HB itself, i.e. here the underlying 14 Gyr SSP appears to have an age  $\sim 5$  Gyr, even without the statistical fluctuations (see Figure 2). Thirdly, the magnitude of the scatter in apparent age caused by the scatter in  $H\beta$  also depends on which diagnostic grid is used and what the properties of the underlying population are. Figure 7 illustrates this last point. In the left hand panel (i.e. the  $H\beta$  vs.  $Fe5406$  grid) it can be seen that the  $Fe5406$  index also has a scatter of around  $\pm 0.1$ , in addition to the scatter in  $H\beta$ . For the extended blue HB case this induces an uncertainty on both the implied age and metallicity of the population. However for the red HB case (model 1), the magnitude of the fluctuations for these 2 indices conspires to scatter the points along a line of constant age, implying no uncertainty on the age. The right hand panel of Figure 7 demonstrates that not all metallicity indicators behave similarly however – in this case, the  $Mgb$  index shows only negligible fluctuations and all the scatter is seen in the  $H\beta$  index, implying an uncertainty of  $\pm 2$ -3 Gyr for the same red HB simulations.

As a guide to the relative significance of fluctuations in various diagnostic indices,  $1\sigma$  variations from the 30 simulations of the extended blue HB case at  $2 \times 10^5 M_\odot$  are tabulated in Table 3 for all 21 Lick indices, plus  $H\delta_F$ ,  $H\gamma_F$  and  $CaII$ .

As might be expected, fluctuations in  $H\beta$  are larger for the  $2 \times 10^4 M_\odot$  case with a scatter of around  $\pm 0.25$ , implying an uncertainty of up to 2 Gyrs on the modelled 3.5 Gyr SSP. It should be noted that, in this case, most of the fluctuations are coming from discrete sampling in the upper portion of the RGB, since the HB consists of a very compact red clump with very little extension.

Results from the  $2 \times 10^6 M_\odot$  simulations are also plotted in Figure 7 but have been arbitrarily shifted to the lower left hand corner of the diagrams for clarity. It can be seen that, even with this total mass, there are still fluctuations in the  $H\beta$  index at the level of  $\sim 0.05$  in EW, corresponding to an uncertainty in age of 0.5-1 Gyr for old SSPs. Various of the metal lines also display low level fluctuations implying a minimum uncertainty of around 0.05 dex in  $[Fe/H]$ . However, for these  $2 \times 10^6 M_\odot$  simulations all indices only fluctuate at a level that is likely to be within the measurement errors for real data.

## 5 SUMMARY AND DISCUSSION

To summarise, we have created integrated spectra for 16 SSPs, 4 each at 4 different metallicities, all with an underlying age of 14 Gyr, with a range of extended HB morphologies. This was done by varying the mass loss prescription for each individual SSP in 2 ways, firstly setting a mean mass,  $\langle M \rangle$ , for stars coming on to the ZAHB, and then adding a spread in mass loss,  $\sigma_M$ . We find that the  $H\beta$  strength for each SSP depends on the exact temperature distribution of stars along the HB, which in turn depends on the exact details of the mass loss prescription coupled with the metallicity of the population in question. For any of the modelled SSPs with any amount of blue HB extension,  $H\beta$  is increased relative to the fixed  $\eta=0.2$  case (i.e. the ‘standard’ models), implying younger ages than the actual SSP age of 14 Gyr. In the worst-case scenario modelled here, a solar metallicity 14 Gyr population with a blue HB which has a peak in its distribution of stars around 9000K, has an implied age of around 2 Gyr from the strength of the  $H\beta$  line.

Our preliminary investigation to identify spectral features which might be capable of breaking the degeneracy between an old SSP with extended blue HB, and a truly intermediate age or young SSP, indicates that the  $CaII$  index defined by Rose (1984) is a very promising candidate, at least for populations with low velocity dispersions, such as extra-galactic globular clusters (but see caveat in the following paragraph). There is also tentative evidence that the  $MgII$  index, in combination with  $Mgb$ , could also be a very useful tracer of hot blue HBs. There are also indications that the UV continuum shortward of the  $MgII$  feature could also potentially be a useful additional tool, although more work is needed to model this part of the spectrum in the required detail. However, it is interesting to note that the extreme blue HB models (i.e. models 3 and 4 presented here) have very strong UV continuum flux, as demonstrated by Figure 4, even at solar metallicity. This supports the idea that



extreme blue HBs can be a significant contributor to the UV upturn identified in old elliptical galaxies (see review by O’Connell 1999).

An important caveat to all the tests and results presented here is that all our models have been created using SSPs, i.e. single age, single metallicity systems. However another scenario which could explain strong  $H\beta$  lines in a predominantly old population would be the presence of a small fraction of very young stars. Although this is not likely to be an issue for globular clusters (Galactic or extra-galactic) it is a possibility which is hard to completely rule out for elliptical galaxies. Preliminary tests with our population synthesis code indicate that adding even a very small percentage ( $<1\%$ ) of a young SSP (300 Myr or less) to a 14 Gyr SSP would significantly strengthen  $H\beta$  and imply an intermediate age, around 5–6 Gyr (see also Serra & Trager 2007). In fact, this scenario of a ‘frosting’ of young stars in an otherwise old stellar population has been explored by Smith et al. (2009) for (apparently) quiescent galaxies in the Shapley supercluster. However, Smith et al. (2009) use the  $\text{CaII}$  index as a tracer of hot stars and, as we have shown here, this index also traces hot HB stars in an SSP. So far we have not identified any completely unambiguous tracers that can distinguish between the 3 scenarios; 1) a small fraction of hot young stars in an otherwise old population, 2) an old SSP with a hot HB, 3) an intermediate age SSP. It seems likely that no single tracer will be able to disentangle these 3 cases and a combination of well understood spectral indices and colours may well be needed – this is the focus of our ongoing investigation.

Another factor potentially linked to extended blue HBs is the presence of a stellar subpopulation with a high helium fraction. Lee et al. (2005) showed that the same level of helium enrichment required to reproduce the bluer main sequence in the massive GC  $\omega$  Centauri would also naturally produce the extreme blue HB stars seen in that cluster. Very recent observational results have provided some evidence for varying helium fractions within individual GCs and there is at least circumstantial evidence linking helium enriched subpopulations to extended blue HBs (see Bragaglia et al. 2010 and references therein). The theoretical support for the HB morphology–enhanced-helium connection is that stars born with a higher helium abundance will display a lower mass at the turn off for a given cluster age. A lower mass at the TO will favour lower mass – hence hotter and bluer – HB stars.

We were able to test the potential impact of a higher helium abundance on our present work by utilising the helium-enhanced isochrones in the BaSTI database in combination with a grid of helium-enhanced spectra, which have been produced for a subsequent paper (Coelho, Salaris & Percival, 2011, in preparation). We chose helium-enhancement at the level  $Y = 0.3$ , for the  $[\text{Fe}/\text{H}] = -0.7$  isochrone, which is a reasonable enhancement over the standard cosmological value, given current observational constraints (e.g. Bragaglia et al. 2010) and our new spectra incorporate the same Fe and He abundance ratios as the isochrones. As a preliminary test, we measured the strength of spectral features in individual spectra for both the standard helium and enhanced helium versions, matching the spectra in  $T_{\text{eff}}$  and  $\log g$ . We found that for all the diagnostic lines considered in this paper, the line strengths are practically indistinguishable for the two

cases, with any differences being less than 1 percent (i.e. within the measurement errors). We also created an integrated spectrum for the  $[\text{Fe}/\text{H}] = -0.7$ , 14 Gyr SSP using the helium-enhanced isochrone in combination with the helium-enhanced spectra. Again we found that the strengths of all the indices under scrutiny here are negligibly different from the standard helium case. We note here that this result is consistent with that of Girardi et al. (2007) who find that a similar level of helium enhancement has a negligible effect on broadband colours.

The important point to stress here is that, whilst enhanced helium is a likely mechanism for producing extended blue HBs, it in no way impacts on the work presented in this study. Our diagnostic models and tests are not intended to predict, *a priori*, the existence of hot HB stars, but rather to find diagnostics which can distinguish their presence in a stellar population from other hot components, such as a young sub-population. Whether a blue HB morphology arises from a large mass loss along the RGB in stars with ‘normal’ helium, or from a more moderate mass loss from stars with higher helium, the resulting integrated spectrum is largely unaffected – the only parameter that matters here is the temperature range of stars on the HB, irrespective of how they have been produced. In fact, the results of our enhanced helium tests, described above, show that enhanced helium has absolutely no impact on the diagnostic indices discussed here, such as  $H\beta$ ,  $\text{MgII}$  and  $\text{CaII}$ , nor on the results of the statistical fluctuations tests discussed below.

Finally, the results of the tests presented here in Section 4.1 demonstrate that several key diagnostic line indices are significantly affected by statistical fluctuations, even in average to large mass GCs. Equally problematic is the fact that not all indices fluctuate at the same level – some are strongly affected, including all the Balmer lines, whilst others are only negligibly affected, such as  $\text{CaII}$  (see Table 3). This is potentially a significant source of uncertainty if full-SED fitting methods are used to derive ages, metallicities and/or star formation histories from integrated spectra, since different features in a spectrum can be giving conflicting best fit parameters. The problem is illustrated in Dias et al. (2010) who present integrated spectra for 14 Magellanic Cloud stellar clusters for which they derive best fit ages and metallicities using 2 different fitting codes, STARLIGHT (Cid Fernandes et al. 2005) and *ULySS* (Koleva et al. 2009), and 3 different sets of SSP models, from Bruzual & Charlot (2003), Le Borgne et al. (2004) (PEGASE-HR) and Vazdekis et al. (2010). Half of the clusters studied have masses in the range  $1 - 2.5 \times 10^4 M_{\odot}$ , which corresponds to the low mass cluster modelled here, in Section 4.1. For several clusters, Dias et al. (2010) find that the results from the different fitting routines and models are completely discrepant. As an example, cluster HW1 yields best-fit ages of 3.2, 5.8, 7.9, 9.0, 9.4 and 10 Gyr from the 6 different combinations of SSPs models and SED-fitting routines, whilst its actual age is known to be around 6 Gyr from isochrone fitting to the CMD. Other clusters are even more unconstrained, yielding ages ranging from  $<1$  Gyr to 10 Gyr for the same cluster. Some of these variations in best fit parameters are likely to be due to systematic uncertainties in stellar parameters inherent within the SSP models themselves (see Percival & Salaris 2009), but statistical fluctuations in the observed spectra are almost certainly contribut-

ing to the problem. Hence we urge caution if these types of stellar clusters are to be used as empirical calibrating objects for various aspects of SPS models.

## ACKNOWLEDGMENTS

We thank PAJ and DXC for useful discussions and comments on an early version of this paper. We also thank editorial staff at MNRAS for their handling of the manuscript.

SMP acknowledges financial support from the Science & Technology Facilities Council (STFC) through a Postdoctoral Research Fellowship.

## REFERENCES

- Bragaglia A., Carretta E., Gratton R., D’Orazi V., Cassisi S., Lucatello S., 2010, *A&A* in press, arXiv:1005.2659
- Brown T. M., Ferguson H. C., 2003, in G. Piotto, G. Meylan, S. G. Djorgovski, & M. Riello ed., *New Horizons in Globular Cluster Astronomy* Vol. 296 of *Astronomical Society of the Pacific Conference Series*, Using M32 to Study Rapid Phases of Stellar Evolution. p. 199
- Bruzual G., Charlot S., 2003, *MNRAS*, 344, 1000
- Cid Fernandes R., Mateus A., Sodré L., Stasińska G., Gomes J. M., 2005, *MNRAS*, 358, 363
- Coelho P., Bruzual G., Charlot S., Weiss A., Barbuy B., Ferguson J. W., 2007, *MNRAS*, 382, 498
- Conroy C., Gunn J. E., White M., 2009, *ApJ*, 699, 486
- Cordier D., Pietrinferni A., Cassisi S., Salaris M., 2007, *AJ*, 133, 468
- Dias B., Coelho P., Kerber L., Barbuy B., Idiart T., 2010, *A&A* in press, arXiv:1002.4301
- Fanelli M. N., O’Connell R. W., Burstein D., Wu C., 1990, *ApJ*, 364, 272
- Girardi L., Castelli F., Bertelli G., Nasi E., 2007, *A&A*, 468, 657
- Koleva M., Prugniel P., Bouchard A., Wu Y., 2009, *A&A*, 501, 1269
- Kotulla R., Fritze U., Weilbacher P., Anders P., 2009, *MNRAS*, 396, 462
- Le Borgne D., Rocca-Volmerange B., Prugniel P., Lançon A., Fioc M., Soubiran C., 2004, *A&A*, 425, 881
- Lee H., Lee Y., Gibson B. K., 2002, *AJ*, 124, 2664
- Lee H., Yoon S., Lee Y., 2000, *AJ*, 120, 998
- Lee Y., Demarque P., Zinn R., 1994, *ApJ*, 423, 248
- Lee Y., Joo S., Han S., Chung C., Ree C. H., Sohn Y., Kim Y., Yoon S., Yi S. K., Demarque P., 2005, *ApJ*, 621, L57
- Maraston C., 2005, *MNRAS*, 362, 799
- Munari U., Sordo R., Castelli F., Zwitter T., 2005, *A&A*, 442, 1127
- O’Connell R. W., 1999, *ARA&A*, 37, 603
- Ocvirk P., 2010, *ApJ*, 709, 88
- Percival S. M., Salaris M., 2009, *ApJ*, 703, 1123
- Percival S. M., Salaris M., Cassisi S., Pietrinferni A., 2009, *ApJ*, 690, 427
- Pietrinferni A., Cassisi S., Salaris M., Castelli F., 2004, *ApJ*, 612, 168
- Pietrinferni A., Cassisi S., Salaris M., Castelli F., 2006, *ApJ*, 642, 797
- Ponder J. M., Burstein D., O’Connell R. W., Rose J. A., Frogel J. A., Wu C., Crenshaw D. M., Rieke M. J., Tripicco M., 1998, *AJ*, 116, 2297
- Reimers D., 1975, *Memoires of the Societe Royale des Sciences de Liege*, 8, 369
- Rose J. A., 1984, *AJ*, 89, 1238
- Schiavon R. P., Caldwell N., Rose J. A., 2004, *AJ*, 127, 1513
- Schiavon R. P., Rose J. A., Courteau S., MacArthur L. A., 2004, *ApJ*, 608, L33
- Schiavon R. P., Rose J. A., Courteau S., MacArthur L. A., 2005, *ApJS*, 160, 163
- Serra P., Trager S. C., 2007, *MNRAS*, 374, 769
- Smith R. J., Lucey J. R., Hudson M. J., 2009, *MNRAS*, 400, 1690
- Trager S. C., Worthey G., Faber S. M., Burstein D., Gonzalez J. J., 1998, *ApJS*, 116, 1
- Vazdekis A., Sánchez-Blázquez P., Falcón-Barroso J., Cenarro A. J., Beasley M. A., Cardiel N., Gorgas J., Peletier R. F., 2010, *MNRAS*, 404, 1639
- Vázquez G. A., Leitherer C., 2005, *ApJ*, 621, 695

This paper has been typeset from a  $\text{\TeX}$ / $\text{\LaTeX}$  file prepared by the author.